Hierarchical Assemblies of Carbon Nanotubes for Ultraflexible Li-Ion Batteries

Shahab Ahmad, Davor Copic, Chandramohan George, and Michael De Volder**

One of the most fascinating paradigm shifts in modern electronics is the fabrication of soft and flexible electronic devices. This development is fueled by a continuous search for more compact and intuitive consumer electronics,[1] medical implants,[2] and the emergence of the "Internet of Things."[3] While considerable progress has been made in the fabrication of flexible and stretchable circuits,[4] radio-frequency identification (RFID) tags,[5] and displays,[6] the flexible batteries needed to power these devices remain challenging.[7] Existing flexible batteries are often too heavy, bulky, and rigid, and require a radical redesign of the battery architecture to address these issues.[8] Here we demonstrate that extremely flexible batteries can be achieved by designing carbon nanotube (CNT) microstructures, which decouple the stress induced during bending in the collector electrode from stress in the energy-storage material (Fe_2O_3 anodes and LNCO cathodes in this work). We found that this battery architecture not only imparts excellent flexibility (bending radius ≈ 300 µm), but also high rate (20 A g^{-1}), cycling stability (over 500 cycles at 1 C with capacity retention over 70%).

The design of highly flexible batteries requires judicious engineering of the electrodes to mitigate stress concentration and crack formation. Recent, progress toward flexible batteries includes the use of polymer substrates,[9] composite membranes,[10] CNT yarns,[11] paper-based electrodes,[12] graphene foams, etc.[8,13] However, many of these designs suffer from fast-capacity decay,[14,15] limited flexibility, poor thermal management, and large weight.[8]

Here, we propose a design where stress in the electrode is localized in the current collector and decoupled from the electroactive region, which remains unstressed during bending. To achieve this, we populate a flexible current collector with microscale 3D structures, which contain the electrochemical active material. In order to remain unstressed as the electrode bends, the base of each active microstructure must be small, and therefore, similar to trees, our microstructures have slender trunk planted in the flexible current collector and a wider crown loaded with electrochemically active nanoparticles. **Figure 1** further illustrates our rationale behind the design of the electrode architecture. Vertically aligned CNT "forests" (Figure 1a) have been reported previously as current collectors for high performance non-flexible batteries. CNTs are promising current collectors for batteries because of their electrochemical stability, excellent electrical and thermal conductivity, and large surface area.[8,16–20] However, when CNT forests are bent, they readily crack (Figure 1e). A solution for this problem is to pattern the electrode material in strips, which allows for flexibility in bending along the direction of the strips, however this leads to the same problems when bending in the direction perpendicular to the strips (Figure 1b). In other words, flexibility in two bending directions requires pillar-like geometries, but even then, the ratio between the bending radius and the pillar base should remain sufficiently high to avoid stress at the interface between the pillars and current collector (see Figure 1c). Therefore, this work focuses on microcones as a novel geometry, combining a slender base for stress reduction and a wide crown for particle loading, as shown in Figure 1d. A further motivation for using cones instead of pillars is that CNT pillars form unpredictable wrinkles during the capillary aggregation steps used in our battery fabrication process (see further).[21] SEM images of plain CNT forests bent to a radius of 3 mm already show cracks (Figure 1e), while microcone electrodes bent to radii as small as 300 µm remain intact (Figure 1f).

Figure 2 depicts the electrode fabrication process, which starts by lithographically patterning catalyst particles into rings from which CNTs are grown by thermal chemical vapor deposition (CVD) (see methods and Figure 2a). The CVD process results in the formation of microcylinders that each consists of thousands of vertically aligned CNTs (Figure 2b). Next, these cylinders are transformed into cones using elastocapillary aggregation (Figure 2c).[21–23] Shortly, this process uses capillary forces to pull the CNTs into a close packing, which results in an overall compaction of the CNT cylinders into cones (Figure 2d and Figure S1, Supporting Information).[22] The cones are then transferred by contact printing[24] to a flexible conductive film (Figure 2e) consisting of poly(vinydlene difluoride) (PVDF), double wall CNTs, and phenyl-C61-butyric acid methyl ester (PCBM) in a ratio (90:5:5), which are thoroughly mixed using a planetary ball mill and cast in ≈15 µm thick films, see methods for details. The flexible film is referred to as PCP (**P**VDF, **C**NT, and **P**CBM) in what follows. A top SEM view (Figure 2i) of the film shows that the CNTs bundle into rafts similar to previous reports,[25] and cross-sectional SEM images (Figure S2, Supporting Information) show a uniform spread of material through the film thickness. Interestingly, our PCP film (1 cm^2) is found to be ≈20 times lighter in weight on comparison with standard Cu-foil current collector (MTI corporation Code EQ-bccf-25 µ) (Figure S3, Supporting Information). Figure 2f,j shows that the CNT cones can be transferred with yields close to 100%. Further, it is important to note that most of the catalyst particles remain

Dr. S. Ahmad, Dr. D. Copic, Dr. C. George,
Dr. M. De Volder
Institute for Manufacturing
Department of Engineering
University of Cambridge
17 Charles Babbage Road, Cambridge CB3 0FS, UK
E-mail: gc495@cam.ac.uk; mfld2@cam.ac.uk

DOI: 10.1002/adma.201600914

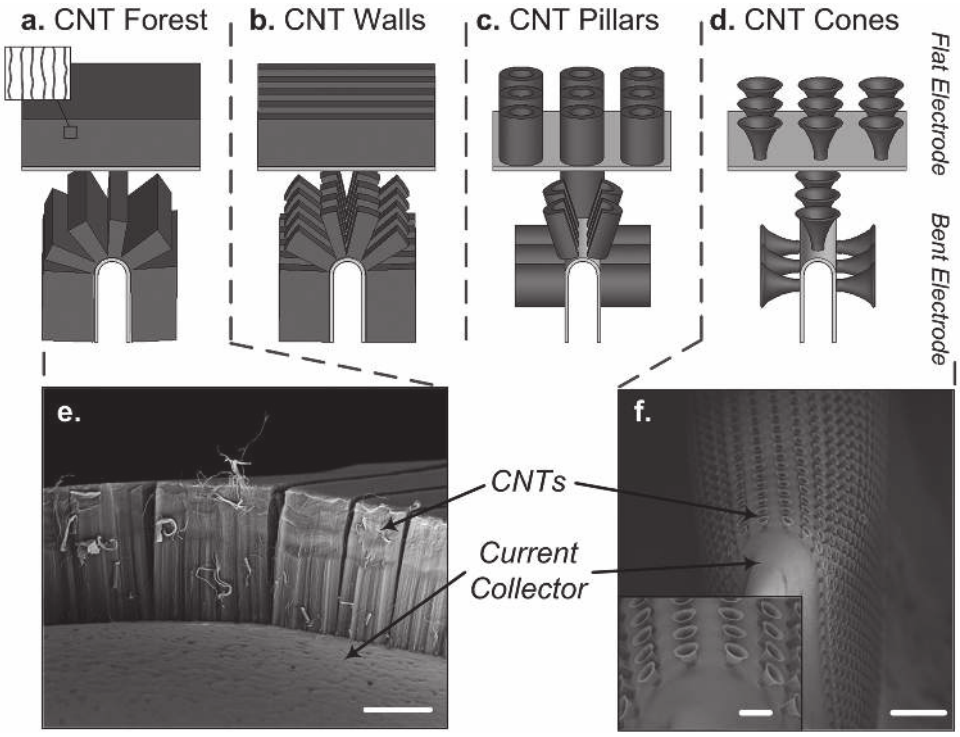

Figure 1. Electrode architectures (top) and their deformation when bent (bottom). a) Unpatterned CNT forest on flat (top) and bent (bottom) substrate. b) CNT forests patterned in strips on flat (top) and bent (bottom) substrate. c) CNT forests patterned in cylinders on flat (top) and bent (bottom) substrate. d) CNT cones on flat and bent substrate. e) Scanning electronic microscopy (SEM) image showing cracks in a CNT forest bent to a radius of 3 mm. Scale bar: 40 μm. f) SEM image of a bent CNT cone electrode. Scale bar: 400 μm. Inset shows the magnified-view SEM image. Scale bar: 100 μm.

attached to the silicon substrate after the CNT transfer printing process, and therefore the Si-substrate can be recycled to synthesize new CNT cones. With our current process the catalyst can be regrown about four times before losing its activity.[26]

Finally, the electrodes are decorated with Fe_2O_3 nanocrystals (≈10 nm diameter, Figure 2g, and Figure S5, Supporting Information) by drop-casting a carefully weighed hexane–Fe_2O_3 suspension. The iron oxide nanocrystals are synthesized by a colloidal method, which involves decomposing iron pentacarbonyl in octadecene in the presence of oleylamine (see methods and Supporting Information).[27] Iron oxide is chosen as the anode material because of its high theoretical capacity (≈1000 mA h g^{-1}), low cost, environmental friendliness, and abundancy.[28,29] In addition, the conversion reactions that take place between Fe_2O_3 and Li ions during charge/discharge cycles require good electrical contact, which is provided by our unique CNT microcone architecture. SEM images of transferred cones on PCP film, loaded with Fe_2O_3 nanoparticles (≈0.5–1 mg) are shown in Figure 2k,l and Figure S4 of the Supporting Information.

The electrodes are packaged, using both standard coin-cells (2032) with Li metal (see methods) and flexible laminated packages using cathodes made using the same CNT cones but decorated using commercial, lithium nickel cobalt oxide powder (LNCO) (Sigma–Aldrich 760986) because Li metal has limited flexibility.[8] In a first series of tests we use the coin cells to compare our hierarchical microcones decorated with Fe_2O_3 to conventional flexible electrodes fabricated by mixing the same Fe_2O_3 nanoparticles with the CNT based PCP film. **Figure 3**a shows that the charge/discharge curves of both electrodes have a sloping plateau at ≈1.8 V corresponding to the first-step lithiation of Fe_2O_3. This becomes more defined at ≈1.2 V with the onset of conversion reaction and at voltages below 1.0 V, the sharp increase of current can be attributed to a full conversion coupled with the formation of a solid electrolyte interface (SEI).[30] These processes can also be seen in the cyclic voltammogram (Figure 3a inset) with a gradual lithiation/delithtaion of Fe_2O_3 at 1.8, 1.2, 0.5, and 2.0 V, in accordance with typical reports on conversion of Fe_2O_3 (i.e., $Fe_2O_3 + 6Li \rightarrow 2Fe + 3Li_2O$).[29,31,32] The peak at 0.7–1.0 V corresponding to Li^+ ion insertion into Fe_2O_3 is more pronounced in the CNT-cone electrodes, suggesting a facile lithiation reaction.

The initial capacity of the CNT cones is ≈1000 mA h g^{-1} at 0.5 C while the conventional electrodes yielded only ≈800 mA h g^{-1} (Figure 3a discharge curves), but in the subsequent cycles the conventional electrode loses more than half of the initial capacity (Figure 3b), while the CNT cone electrodes remarkably retain more than 70% of their initial capacity. At high current densities (rates), CNT cone electrodes clearly outperform the capacity and retention of the conventional flexible electrodes (Figure 3b). For instance, the capacity of conventional electrodes quickly fades and reaches values close to 0 mA h g^{-1} at a rate of 7 C (Figure 3b), which indicates poor electrochemical activities while the microcone electrodes maintain more than 300 mA h g^{-1} under the same conditions. Such drop in performance of conventional electrodes where the metal oxide is blended in a polymer binder was also reported previously.[33] In comparison, the CNT cone electrodes still yielded appreciable capacity at 10, 15, and 20 C (Figure 3c), and despite these harsh

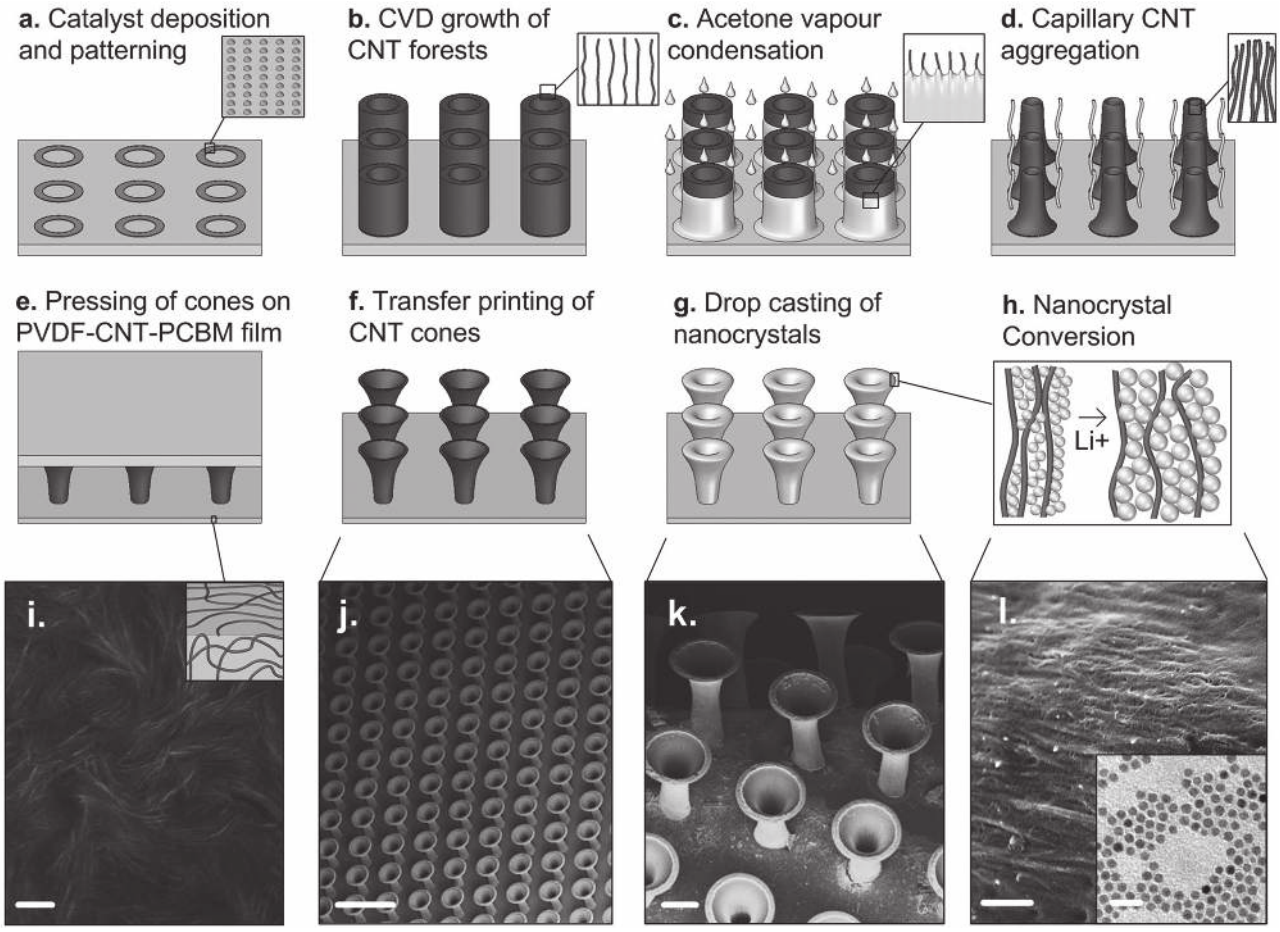

Figure 2. Fabrication process schematics and characterizations. a) Photolithographically patterned Fe catalyst film deposited by e-beam evaporation (inset shows formation of nanostructured Fe islands after hydrogen annealing at 800 °C). b) CNT cylinders grown by CVD. c) Capillary aggregation by acetone vapours. d) Aggregated CNT cones. e) Transfer-printing of CNT cones on the flexible PCP film. f) Transferred CNT cones PCP film. g) Drop-casting of Fe_2O_3 nanocrystals. h) Close-up view of the Fe_2O_3 coating. i) Top-view SEM image of flexible CNT–polymer PCP film. Scale bar: 200 nm. j) SEM image of transferred CNT-cone-structure assemblies. Scale bar: 200 μm. k) SEM image of bent electrode coated with Fe_2O_3 nanocrystals. Scale bar: 40 μm. l) SEM image of the Fe_2O_3 nanocrystals coating. Scale bar: 500 nm. The inset shows a transmission electron microscopy (TEM) image of the iron oxide nanocrystals. Scale bar: 20 nm.

high rate tests, the electrodes still exhibited sustained capacities 650–800 mA h g^{-1} when the rate was reduced to 0.5 C. We initially observed a difference in charge and discharge capacity after reverting from high to low rate, which might be due to the binder free nature of our electrode architecture and the thick deposition of active particles built up of multiple layers. The cone architecture therefore not only imparts excellent flexibility, but also enhances battery performance substantially. Because the cones bring the active material outside of the binder, the electrochemical reactions take place at the surface of the CNT cones. This protects the collector electrode from the deleterious side reactions between active materials (Fe, Li_2O, and Fe_2O_3) and binder molecules, which can lead to large internal resistance. Furthermore, the developed CNT cones are able to accommodate the drastic volume change[34] taking place during conversion reactions, and ensure good contact to the active material resulting in the observed higher charge retention, also compared to other recently published CNTs-metal oxide electrodes.[33,35,36] Finally, the cone electrodes were cycled 500 times at 1 C with no appreciable change in the capacity as shown in Figure 3d, and, in Table S1 in the Supporting Information, we further compare the performance of our battery to those based on CNT forests previously reported.

Finally, we have constructed flexible full cells with both CNT cone anodes and cathodes, as depicted in the schematics of **Figure 4**a. The former is coated with Fe_2O_3 as discussed above, and the cathode with commercial LNCO powder (see methods). Figure 4b shows the charge/discharge curves from the full cell. The full cells were folded multiple times and then tested in flat state, they operate around 3.1 V with a sloping plateau between 4.0–2.0 V and the capacity was stabilized after the second cycle (for LNCO), and delivers a reversible capacity of ≈120 mA h g^{-1} at 2 C (Figure 4b). Figure S6 of the Supporting Information shows further cycling data of the battery while it is being bent and released for 15 cycles. These batteries were connected to a white light emitting diode (LED, 3 V) and flexed to radii of about 3 mm while powering the LED as illustrated in Figure 4c. The bending radius is currently limited by the

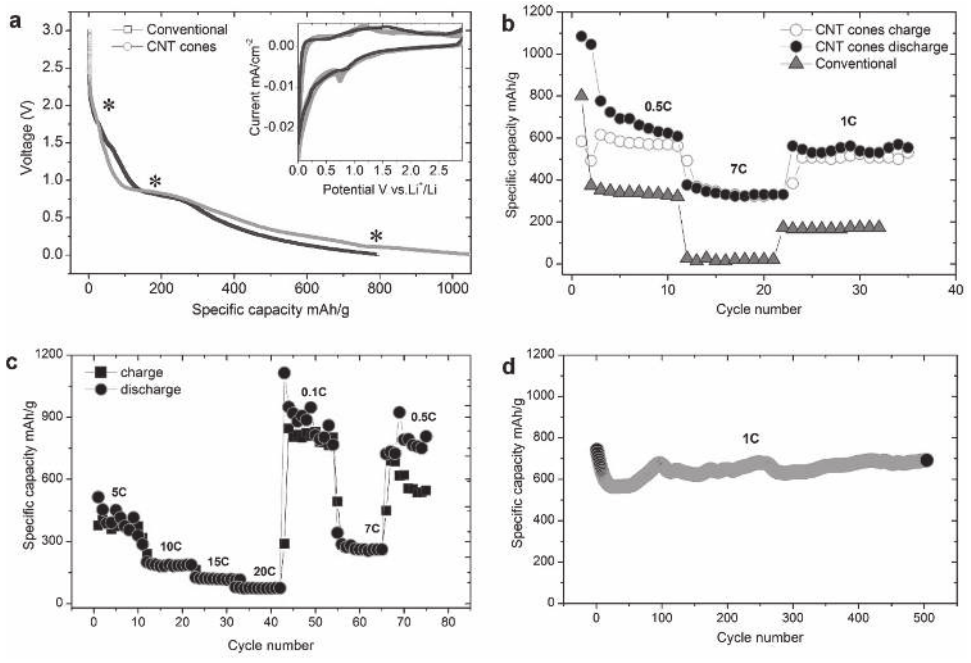

Figure 3. Electrochemical performance comparison of CNT cones-Fe_2O_3 and conventional electrodes with Fe_2O_3. a) Discharge cycles, and cyclic voltammetry at 0.5 mV s^{-1} (inset). b) Cycling performance of both microcone and conventional flexible electrodes. c) High rate performance of the CNT cone electrodes. d) Extended lifetime testing of the CNT cone electrodes at 1 C rate for 500 cycles.

packaging rather than the electrodes themselves (more information in Supporting Information). Finally, complex electrode architectures are often not able to survive the harsh battery cycling conditions. Therefore, we opened our flexible cells after 1000 cycles, which corresponds to the lifetime of the battery to image the CNT cones. Figure 4e reveals that the overall cone morphology is well maintained, similar to as fabricated CNT cones shown in Figure 4d. We believe this is because the cones are well anchored in the collector electrode, and because capillary aggregated CNT structures are substantially more resilient than as-grown forests.[21]

In conclusion, this paper presents a new electrode architecture, which consists of hierarchical cone shaped CNT structures with a slender trunk embedded in a flexible light weight collector electrode and a wide crown that is loaded with nanocrystals for energy storage. This architecture allows the electrodes to be folded to very small radii without inducing stress in the active material network. These unique electrodes not only alleviate stress, but also bring the active particles outside of the binder, which dramatically enhances the performance of the conversion reactions. This results in batteries that are extremely flexible (300 µm radii) and at the same time offers excellent rates (as high as 20 A g^{-1}), and cyclability (over 500 cycles at 1 C with capacity retention >70%).

Experimental Section

Lithography: Clean (100) silicon wafers were first dehydrated at 200 °C, and coated with an adhesion promoter (Ti-prime). Then AZ 4533 photoresist was spin coated (3000 rpm, 30 s) and prebaked at 115 °C for 2 min on a hot plate, and exposed. The patterns were developed in diluted AZ 351B (1:4 DI water, 3 min), followed by rinsing in deionized (DI) water and blow-drying.

CNT Growth: E-beam evaporation was used to deposit a 10 nm Al_2O_3 and 1 nm Fe catalyst film. The Si-wafers were then diced and the catalyst was patterned by lift-off. Next, CNT forests were grown in cylindrical structures by thermal CVD in a horizontal tube furnace at atmospheric pressure, with flows of 100/400/100 sccm C_2H_4/H_2/He, at 800 °C. The CNTs were rapidly cooled in the growth atmosphere before purging the CVD chamber with helium.

Densification, PCP Film Fabrication, and Transfer Printing: The cylindrical CNT microstructures were converted into elongated cone-like structures by a capillary forming process, reported previously.[22] These CNT microcones were transferred onto the flexible PCP film, which was fabricated as follows: 15 mg of methanofullerene phenyl C61 butyric acid methyl ester (PCBM) was dissolved in 3 mL dimethylformamide (DMF) and ultrasonicated for 1 h. 15 mg double-wall carbon nanotubes (DWCNTs) (Nanocyl NC2000) were added to the PCBM solution and ultrasonicated for 30 min. A solution of poly(vinylidene fluoride) (PVDF) (300 mg in 3 mL DMF) was added as binder to the CNT-PCBM solution and stirred. Finally, the PVDF–CNT–PCBM suspension was ball milled (planetary) in a grinding jar (25 mL) with a single metal ball for 2 h with an interval of 30 s after every 2 min. The ball-milled PCP suspension was drop-cast over a clean soda-lime glass slide. The temperature of the glass substrate was increased to 60 °C to dry the film and was then raised to 175 °C to soften the PVDF. The densified CNT cones were then transferred on the PCP film by microcontact printing.[24]

Nanocrystal Synthesis and Coating: Iron oxide (Fe_2O_3) nanocrystals were synthesized by a colloidal method, which involved decomposing iron pentacarbonyl ($Fe(CO)_5$) (≈1–2 mL) in octadecene (≈20 mL) in the presence of an oleylamine and oleic acid mixture (≈1.5 mL) as reported previously.[27] More synthesis details are provided in the Supporting Information, along with an XRD scan (Figure S5, Supporting Information). Purified iron oxide nanoparticles, suspended in hexane, were drop-cast onto the CNT microstructures at 40 °C. The substrate was left in air for a few minutes to completely evaporate the solvent. The PCP film with CNT microstructures was then peeled-off from the glass substrate. The flexible electrode was tested in half cells with 2032 coin

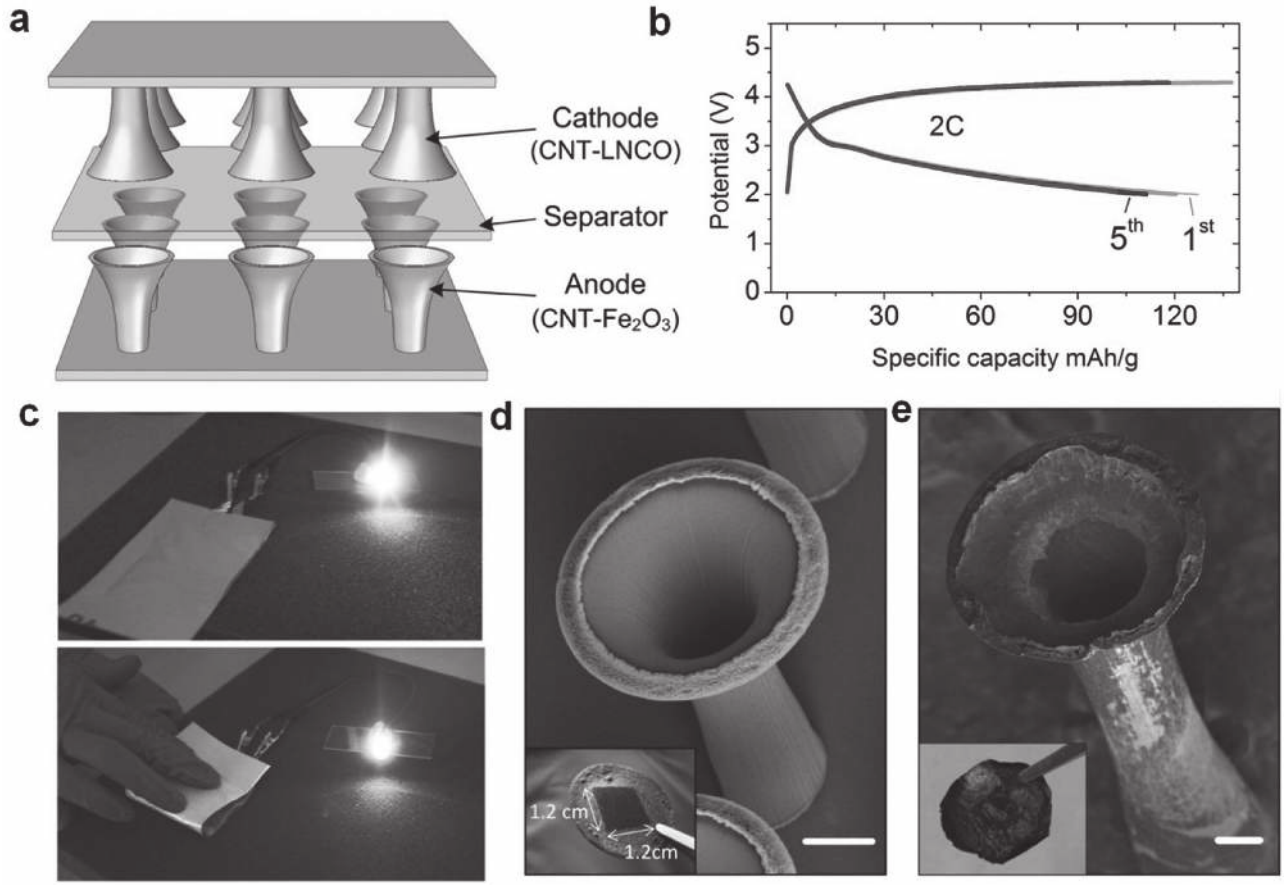

Figure 4. Full flexible cell fabrication and characterizations. a) Schematic representation of the full cell with a CNT cone anode and cathode. b) Charge/discharge curves of full cell: iron oxide–CNT cones and LNCO–CNT cones at 2C (first and fifth cycles indicated). c) Flexible CNT cone battery connected to a 3 V white-light LED. d) SEM image of CNT cone, taken at 35° tilt angle, before testing in a full cell. The inset shows 1.2 cm × 1.2 cm area coverage of transferred CNT cones on PCP film. Scale bar: 20 μm. e) SEM image of CNT cone, taken at 40° tilt angle, and picture of the electrode (inset) after 1000 charge/discharge cycles and repeated bending of the electrode. Scale bar: 10 μm.

type casings with pure Li metal as the reference and counter electrodes, and was separated by a layer of polypropylene (PP). 1 M $LiPF_6$ served as the electrolyte. The battery fabrication and equilibration of cells were carried out in an argon (Ar) filled glovebox at room temperature. The full cells were fabricated by drop-casting Fe_2O_3 nanoparticles and commercial LNCO powder (from Aldrich 760986, <0.5 μm) on CNT cone electrodes. These were separated by a polypropylene layer or Whatman borosilicate paper soaked with 1 M $LiPF_6$ as electrolyte, and the pack was laminated in an Ar filled glovebox.

Conventional Electrode Fabrication: For comparison, conventional flexible electrodes were fabricated by adding the required amount of Fe_2O_3 nanoparticles (in hexane or chloroform) to 1–3 mL of presynthesised and ball-milled PCP suspension (DMF). The composite suspension was sonicated and then stirred for 1 h each before drop-casting into film and packaging the battery in the same way as described above.

Supporting Information

Supporting Information is available from the Wiley Online Library or from the author.

Acknowledgements

S.A. and M.D.V. acknowledge the EPSRC First Grant MUSCAN nr EP/L025531/1. M.D.V. and C.G. acknowledge ERC starting grant 337739-HIENA and the Marie Curie CIG Grant 618250-CANA. S.A., D.C., C.G., and M.D.V. acknowledge fruitful discussion and help from S. Engelke.

Received: February 16, 2016
Revised: March 24, 2016
Published online: May 17, 2016

[1] T. Someya, *Nat. Mater.* **2010**, *9*, 879.
[2] R. C. Webb, A. P. Bonifas, A. Behnaz, Y. Zhang, K. J. Yu, H. Cheng, M. Shi, Z. Bian, Z. Liu, Y.-S. Kim, W.-H. Yeo, J. S. Park, J. Song, Y. Li, Y. Huang, A. M. Gorbach, J. A. Rogers, *Nat. Mater.* **2013**, *12*, 938.
[3] Y. Zhan, Y. Mei, L. Zheng, *J. Mater. Chem. C* **2014**, *2*, 1220.
[4] J. A. Fan, W.-H. Yeo, Y. Su, Y. Hattori, W. Lee, S.-Y. Jung, Y. Zhang, Z. Liu, H. Cheng, L. Falgout, M. Bajema, T. Coleman, D. Gregoire, R. J. Larsen, Y. Huang, J. A. Rogers, *Nat. Commun.* **2014**, *5*, 3266.
[5] J. A. Rogers, T. Someya, Y. Huang, *Science* **2010**, *327*, 1603.
[6] J. A. Rogers, *Science* **2001**, *291*, 1502.
[7] H. Nishide, K. Oyaizu, *Science* **2008**, *319*, 737.
[8] X. Wang, X. Lu, B. Liu, D. Chen, Y. Tong, G. Shen, *Adv. Mater.* **2014**, *26*, 4763.
[9] M. S. Jung, J. H. Seo, M.-W. Moon, J. W. Choi, Y. C. Joo, I.-S. Choi, *Adv. Energy Mater.* **2015**, *5*, 1400611.

[10] N. B. Aetukuri, S. Kitajima, E. Jung, L. E. Thompson, K. Virwani, M.-L. Reich, M. Kunze, M. Schneider, W. Schmidbauer, W. W. Wilcke, D. S. Bethune, J. C. Scott, R. D. Miller, H.-C. Kim, *Adv. Energy Mater.* **2015**, *5*, 1500265.
[11] J. Ren, Y. Zhang, W. Bai, X. Chen, Z. Zhang, X. Fang, W. Weng, Y. Wang, H. Peng, *Angew. Chem. Int. Ed.* **2014**, *53*, 7864.
[12] L. Hu, H. Wu, F. La Mantia, Y. Yang, Y. Cui, *ACS Nano* **2010**, *4*, 5843.
[13] N. Li, Z. Chen, W. Ren, F. Li, H.-M. Cheng, *Proc. Natl. Acad. Sci. USA* **2012**, *109*, 17360.
[14] V. L. Pushparaj, M. M. Shaijumon, A. Kumar, S. Murugesan, L. Ci, R. Vajtai, R. J. Linhardt, O. Nalamasu, P. M. Ajayan, *Proc. Natl. Acad. Sci. USA* **2007**, *104*, 13574.
[15] B. J. Landi, M. J. Ganter, C. M. Schauerman, C. D. Cress, R. P. Raffaelle, *J. Phys. Chem. C* **2008**, *112*, 7509.
[16] S. H. Choi, J.-H. Lee, Y. C. Kang, *ACS Nano* **2015**, *9*, 10173.
[17] J. Liu, K. Song, P. A. van Aken, J. Maier, Y. Yu, *Nano Lett.* **2014**, *14*, 2597.
[18] X. Jia, Y. Kan, X. Zhu, G. Ning, Y. Lu, F. Wei, *Nano Energy* **2014**, *10*, 344.
[19] M. De Volder, S. H. Tawfick, R. H. Baughman, A. J. Hart, *Science* **2013**, *339*, 535.
[20] J. Chen, Y. Liu, A. I. Minett, C. Lynam, J. Wang, G. G. Wallace, *Chem. Mater.* **2007**, *19*, 3595.
[21] a) M. De Volder, S. J. Park, S. H. Tawfick, D. O. Vidaud, A. J. Hart, *J. Micromech. Microeng.* **2011**, *21*, 045033; b) M. De Volder, A. J. Hart, *Angew. Chem. Int. Ed.* **2013**, *52*, 2412.
[22] M. De Volder, S. H. Tawfick, S. J. Park, D. Copic, Z. Zhao, W. Lu, A. J. Hart, *Adv. Mater.* **2010**, *22*, 4384.
[23] Y. Hayamizu, T. Yamada, K. Mizuno, R. C. Davis, D. N. Futaba, M. Yumura, K. Hata, *Nat. Nanotechnol.* **2008**, *3*, 289.
[24] Z. Rong, Y. Zhou, B. Chen, J. Robertson, W. Federle, S. Hofmann, U. Steiner, P. Goldberg-Oppenheimer, *Adv. Mater.* **2014**, *26*, 1456.
[25] J. Wu, L. Jiao, A. Antaris, C. L. Choi, L. Xie, Y. Wu, S. Diao, C. Chen, Y. Chen, H. Dai, *Small* **2013**, *9*, 4142.
[26] M. De Volder, S. Tawfick, S. J. Park, A. J. Hart, *ACS Nano* **2011**, *5*, 7310.
[27] C. George, D. Dorfs, G. Bertoni, A. Falqui, A. Genovese, T. Pellegrino, A. Roig, A. Quarta, R. Comparelli, M. L. Curri, R. Cingolani, L. Manna, *J. Am. Chem. Soc.* **2011**, *133*, 2205.
[28] J. S. Chen, T. Zhu, X. H. Yang, H. G. Yang, X. W. Lou, *J. Am. Chem. Soc.* **2010**, *132*, 13162.
[29] M. V. Reddy, T. Yu, C. H. Sow, Z. X. Shen, C. T. Lim, G. V. Subba Rao, B. V. R. Chowdari, *Adv. Funct. Mater.* **2007**, *17*, 2792.
[30] A. Paolella, R. Brescia, M. Prato, M. Povia, S. Marras, L. De Trizio, A. Falqui, L. Manna, C. George, *ACS Appl. Mater. Interfaces* **2013**, *5*, 2745.
[31] Q. Su, D. Xie, J. Zhang, G. Du, B. Xu, *ACS Nano* **2013**, *7*, 9115.
[32] B. Tian, J. Świątowska, V. Maurice, S. Zanna, A. Seyeux, L. H. Klein, P. Marcus, *J. Phys. Chem. C* **2013**, *117*, 21651.
[33] A. Goyal, A. L. M. Reddy, P. M. Ajayan, *Small* **2011**, *7*, 1709.
[34] C. Kim, S. Choi, S. Yoo, D. Kwon, S. Ko, J.-M. Kim, S.-Y. Lee, I. D. Kim, S. Park, *Nanoscale* **2015**, *7*, 11286.
[35] J. Lee, C. Jo, B. Park, W. Hwang, H. I. Lee, S. Yoon, J. Lee, *Nanoscale* **2014**, *6*, 10147.
[36] G. Zhou, D. W. Wang, P. X. Hou, W. Li, N. Li, C. Liu, F. Li, H.-M. Cheng, *J. Mater. Chem.* **2012**, *22*, 17942.